THE
AUSTRALIAN
NATIONAL
UNIVERSITY

RESEARCH SCHOOL OF PHYSICAL SCIENCES

ANU-P/1107
November 1992

Charge-Exchange Reactions on ^{36}S

L.K. Fifield, W.N. Catford, N.A. Orr and T.R. Ophel

Department of Nuclear Physics, Research School of Physical Sciences and Engineering, Australian National University, GPO Box 4, Canberra ACT 2601, Australia

A. Etchegoyen and M.C. Etchegoyen

TANDAR, Departamento de Fisica, CNEA
Av del Libertador 8250, 1429 Buenos Aires, Argentina

INSTITUTE OF ADVANCED STUDIES

Accepted for publication in
Nuclear Physics A
November 1992

Charge-Exchange Reactions on ^{36}S

L.K Fifield, W.N.Catford, N.A.Orr, and T.R.Ophel
Department of Nuclear Physics, Research School of Physical Sciences and Engineering, Australian National University, GPO Box 4, ACT 2601, Australia

A. Etchegoyen* and M.C. Etchegoyen*
TANDAR, *Departamento de Física, CNEA*
Av. del Libertador 8250, 1429 Buenos Aires, Argentina

A series of charge-exchange reactions on ^{36}S targets have been investigated at beam energies ~7 MeV/A. Pronounced selectivities to different final states in ^{36}P are observed which depend on the projectile employed. An interpretation of the data in terms of one- and two-step pictures of the reaction mechanism is presented. At least two, and probably all, of the reactions have a significant 1-step contribution to the reaction mechanism at these energies.

Nuclear Reactions: $^{36}S(^{7}Li,^{7}Be)$, $(^{11}B,^{11}C)$, $(^{13}C,^{13}N)$, $(^{18}O,^{18}F)$, E(^{7}Li) = 54 MeV, E(^{11}B) = 81 MeV, E(^{13}C) = 94.5 MeV, and E(^{18}O) = 124 MeV. Measured $\sigma(\theta,E_x)$, deduced reaction mechanism. Also $^{36}S(^{13}C,^{13}C)$, $(^{18}O,^{18}O)$, elastic scattering, E(^{13}C) = 98 MeV, E(^{18}O) = 112 MeV. Deduced optical potentials.

1. INTRODUCTION

The recent interest in charge-exchange reactions induced by heavy-ions has been motivated principally by the possibility of studying states that are inaccessible to the more frequently used (p,n) reactions. Studies have been performed[1-4] over a wide spectrum of energies from 5 to 100 MeV/A, with a trend towards higher energies. This trend has been motivated by the increasing dominance of one-step over two-step processes with increasing energy due to the rapid decrease of the two-step contribution[5] in contrast to the slowly decreasing contribution from the $\sigma.\tau$ part of the nucleon-nucleon force[6]. Nevertheless, there is some evidence that one-step processes may still be important relative to the two-step processes even at energies as low as 5 MeV/A[7]. In the present work, four charge-exchange reactions on ^{36}S targets have been studied at energies of 5-8 MeV/A in order to probe the reaction mechanism at these energies and to obtain spectroscopic information on the neutron-rich residual nucleus ^{36}P.

The original motivation for the present work came from earlier studies of charge-exchange reactions on ^{36}S targets[8,9] which were directed towards measuring the mass and low-lying level-scheme of the $N = 21$ nucleus ^{36}P. Measurements were performed at the Australian National University employing the $(^{7}Li,^{7}Be)$ and $(^{11}B,^{11}C)$ reactions[8] and at Munich using the $(^{14}C,^{14}N)$ reaction[9]. The two determinations of the ground state mass were in excellent agreement, and each laboratory observed only a single excited state. However, the excitation energies of these excited states were clearly different: a state at 0.45 MeV was populated by the $(^{14}C,^{14}N)$ reaction, whereas the excitation energy of the state populated by both the $(^{7}Li,^{7}Be)$ and $(^{11}B,^{11}C)$ reactions was 0.25 MeV. A subsequent high resolution study[10] of the γ-rays emitted following the β decay of ^{36}Si has confirmed the existence of the two states, and provided more accurate estimates of their excitation energies, viz 0.250 and 0.425 MeV. The question then arose as to whether this selectivity of the different charge-exchange reactions could be used to throw light on the reaction mechanism, and in particular on the interplay between one- and two-step processes. In order to investigate this question further, new measurements of the $(^{7}Li,^{7}Be)$ and $(^{11}B,^{11}C)$ reactions with much lower backgrounds have been carried out using very pure implanted ^{36}S targets, and the $^{36}S(^{13}C,^{13}N)^{36}P$ and $^{36}S(^{18}O,^{18}F)^{36}P$ reactions have

been investigated for the first time.

2. EXPERIMENTAL DETAILS

Beams of ^{7}Li, ^{11}B, ^{13}C and ^{18}O were obtained from the 14UD Pelletron accelerator at the Australian National University. These were used to bombard high-purity ^{36}S targets which had been prepared by implanting negative ions of ^{36}S into thin carbon foils. Typically, these targets contained $10\mu g/cm^2$ of ^{36}S in 30 $\mu g/cm^2$ of carbon and the ^{36}S constituted 96% of the isotopes other than carbon and oxygen in the target. The remaining 4% consisted predominantly of ^{35}Cl and ^{34}S in the ratio 3:1. Details of the fabrication and characterisation of these targets may be found in ref.[11]. Reaction products were momentum analysed by an Enge split-pole magnetic spectrometer and detected at the focal plane in a multi-element gas-filled heavy-ion detector. Experimental parameters for the four reactions are listed in table 1.

In addition to the charge-exchange reaction data, elastic scattering angular distributions were me sured with the ^{13}C and ^{18}O beams, at energies of 98 and 112 MeV respectively, in order to define the optical model parameters to be used in DWBA calculations of the one-step process. Measurements were made with the spectrometer positioned at laboratory angles from 4° to 20° in steps of 1° with an angular acceptance in the reaction plane of 0.1°. The data at each angle were normalised to the yield of ions elastically scattered from ^{36}S into a silicon detector positioned at $-15°$ to the beam direction.

3. RESULTS

3.1. Charge-Exchange Reactions

Spectra for the four charge-exchange reactions studied in the present work are presented in fig.1. For completeness, a representation of the $(^{14}C,^{14}N)$ data of Meyer et al. is also shown. Cross-sections (averaged over the angular acceptance of the spectrometer) in the laboratory frame are given in table 2.

As foreshadowed in the Introduction, there is considerable variation in the selectivity for different final states in ^{36}P among the five reactions, with three different patterns discernible. The $(^{13}C,^{13}N)$ reaction is seen to follow

the same pattern as the (^7Li,^7Be) and (^{11}B,^{11}C) reactions, whereas the (^{18}O,^{18}N) and (^{14}C,^{14}N) spectra are each distinctively different from all the others. Note that, with the considerable reduction in background and improved resolution relative to the earlier measurements, it is now possible to see that the 425 keV level is populated, albeit weakly, by the (^{11}B,^{11}C) reaction. However, the observation of this level in the (^7Li,^7Be) reaction is precluded by the presence of the Doppler-broadened peak due to the 429 keV level in ^7Be.

3.2. Elastic Scattering Angular Distributions

The elastic scattering angular distributions are shown in fig. 2. Optical model parameters were deduced from the fitting procedure with the computer code **PTOLEMY**. Several searches resulted in a number of different sets of parameters, but the one-step charge-exchange calculations were found not to depend strongly on the set used. Table 3 lists the parameters used in the present work, and the corresponding fits are also shown in fig. 2. These potentials were used for both entrance and exit channels.

4. DISCUSSION

4.1. The Structure of ^{36}P: Shell Model Calculations

Recently, it has become possible to perform shell model calculations for nuclei near the N=20 shell closure with nucleons occupying both the *sd* and *fp* major shells. A number of such calculations have been published with the aims both of understanding the origin of the transition from spherical to deformed shapes which takes place in this mass region at Z ~13[12], and of interpreting the recently acquired wealth of β^- decay data for the more neutron-rich nuclei. These calculations employed a new $sd-fp$ shell interaction, appropriately termed **SDPF**, which includes the $1d_{5/2}$, $2s_{1/2}$, $1d_{3/2}$, $1f_{7/2}$, $2p_{3/2}$, $1f_{5/2}$ and $2p_{1/2}$ model space and is described in detail in ref.[13]. In the present work, this **SDPF** interaction has been used to calculate the

required properties of states in ^{36}P and ^{36}S since it gives a good description of the above-mentioned β^- decays and, in particular, of $^{36}P(\beta^-)^{36}S$. The (6-16)2BME interaction of Cohen and Kurath[14] was used for the p-shell projectile/ejectile systems, and the universal sd shell (USD) interaction of Wildenthal[15] was used for ^{18}O and ^{18}F. The calculations were performed with the computer code OXBASH[16].

It is expected that the low-lying level scheme of ^{36}P, which has a single neutron outside the closed $N = 20$ shell, should be well described by a simple weak-coupling scheme in which a single $2s_{1/2}$ proton may be coupled to either a $1f_{7/2}$ neutron to give a low-lying 3^-, 4^- doublet, or to a $2p_{3/2}$ neutron to give 1^- and 2^- states. This expectation is largely borne out by the detailed shell model calculations performed in the present work (see table 4). The one exception is the 2^- state which, in addition to the expected major contribution from a $2p_{3/2}$ neutron coupled to a $2s_{1/2}$ proton, has a significant contribution from a $1f_{7/2}$ neutron coupled to a $1d_{3/2}$ proton.

The calculations predict a 4^-, 3^- doublet at 0 and 135 keV, respectively, and a 2^- state at 665 keV in excitation. The 1^- member is predicted at 1.56 MeV. Warburton and Becker's[17] shell model interpretation of the $^{36}P(\beta^-)^{36}S$ data strongly suggests that the ^{36}P ground state does indeed have $J^\pi = 4^-$. It follows that a reasonable interpretation of the charge-exchange and γ-ray data is that the 250 and the 425 keV levels are the expected low-lying 3^- and 2^- states respectively.

On the basis of this interpretation of the observed level scheme of ^{36}P, it appears that the unnatural-parity $[\pi = (-1)^{J+1}]$ 4^- ground state is populated strongly by all five reactions, whereas the natural parity 3^- state is populated strongly by only those reactions involving mirror projectile-ejectile systems. The latter observation already hints at a 1-step mechanism because it is only for these 3 reactions that the isospin-flip interaction can contribute to 1-step population of the 3^- state. In contrast, the $(^{14}C,^{14}N)$ and $(^{18}O,^{18}F)$ reactions can populate the 3^- state via only the spinflip-isospin flip component of the nucleon-nucleon interaction.

Nevertheless, the 2-step mechanism was expected *a priori* to be important at the energies employed in the present work, and in the following sections we explore the similarities and differences between the 2-step and 1-step predictions.

4.2. Two-Step Calculations

In a recent paper[18], Brink's semi-classical theory[19] of (single-step) heavy-ion induced transfer reactions has been extended to two-step processes. In the present work we have carried out calculations within this framework for each of the reactions studied here. Details of the calculations may be found in ref.[18], but for present purposes the essential assumptions are:

i) Nucleons are transferred between definite shell-model orbitals in both target and projectile.

ii) The reaction takes place on a very short time scale, ($\approx 10^{-22}s$) due to the very short time that the interacting nuclei spend within the range of the nuclear forces. This has the following consequences:

a) The order in which the two transfers take place can not be important, because the two steps take place essentially simultaneously.

b) The Q-values of the individual steps of the reaction are not well defined, having an uncertainty of ≈ 5 MeV associated with the short time scale of the reaction. Hence it is necessary to average over a range of Q-values for the first and second steps with the constraint that the sum of the two Q-values be constant.

c) The intermediate states are not physical states of the equilibrated nuclei which would result if the reaction terminated after the first step (for example, ^{37}S and ^{6}Li or ^{35}P and ^{8}Be in the case of the ^{36}S(^{7}Li,^{7}Be)^{36}P reaction), but rather should be viewed as the ground state of the target or projectile plus or minus a nucleon in a definite shell model orbit.

iii) It should be emphasized that this approach permits the calculation of only the relative populations of different states in the same reaction. Further, it should be borne in mind that the 2-step predictions are for total cross-sections, whereas the experimental data are averages of the differential cross-section over a limited range of angles. This constitutes an additional source of uncertainty in the comparison between the data and the 2-step predictions.

Relative cross sections for the $4^-, 3^-$ and 2^- states in ^{36}P have been calculated within this framework for each of the five reactions studied, and are compared with the experimental results in fig. 3. Although the calculations succeed in reproducing the trends of the data for the (^7Li,^7Be), (^{11}B,^{11}C), and (^{14}C,^{14}N) reactions, and in particular, give a good account of the difference in selectivity to the 0.25 MeV 3^- level between the first two reactions and the third, they fail completely to account for the relative intensities observed in the (^{13}C,^{13}N) and (^{18}O,^{18}F) reactions, where the predicted intensities of the 2^- state are in anti-phase with the experimental observations.

It is useful to look more closely at the factors which influence the relative transition rates of these two-step processes.

(a) Angular and linear momentum conservation favour one-step transitions from shell model orbits with $j=\ell+\frac{1}{2}$ ($j_>$) to orbits with $j=\ell-\frac{1}{2}$ ($j_<$) or vice versa. In such cases, the transition probability is dominated by the transitions between $|m_j|$=j substates[19].

In the present work, this favoured situation applies only in the neutron stripping step of the (^{13}C,^{13}N) and (^{14}C,^{14}N) reactions where the neutron is transferred from the $p_{1/2}$ orbit to either the $f_{7/2}$ or $p_{3/2}$ orbits. On the basis of the simple physical argument given below, it is then possible to understand why the two-step calculations favour population of the 4^- state over the 3^- state in these two reactions.

The preferred process is depicted schematically in fig. 4 for the (^{13}C,^{13}N) reaction. Consider first the neutron stripping step (arbitrarily chosen to be step A) shown in fig. 4a. The transition probability is a maximum for the trajectory shown. For this trajectory, the orbital angular momentum of the transferred nucleon is perpendicular to the reaction plane and in opposite senses before and after the transfer, while the spin projection is unchanged. Hence the transition proceeds from the $m_j = +\frac{1}{2}$ substate in the projectile to the $m_j = -\frac{7}{2}$ substate in the intermediate nucleus. Transfer of a neutron with the opposite spin projection, and hence with the opposite sense of the orbital angular momentum, is not favoured because of the direction of relative motion of the two nuclei.

In the second (proton-pickup) step, the relative motion favours the trajectory shown in fig. 4b and hence the transfer of the spin-up member of the pair of $2s_{\frac{1}{2}}$ protons, because the transfer takes place to the $1p_{\frac{1}{2}}$ orbit for which the spin and orbital projections must be anti-parallel. It follows

that it is the spin-down proton which is left behind in what is now ^{36}P. The coupling of its angular momentum to that of the $m_j = -\frac{7}{2}$ neutron results in a projection of the total spin M_J=–4. Hence, the process depicted in fig. 4 produces the 4^- state in ^{36}P, but not the 3^- state. Production of the 3^- state proceeds by a less favoured route, and the transition probability is reduced by about an order of magnitude as a result. The argument is essentially unchanged for the (^{14}C,^{14}N) reaction despite the difference in spin between the projectile and ejectile systems in this case.

(b) For the other three reactions, the neutron stripping path is $j_>$ to $j_>$ and transitions between $|\, m_j \,| \neq j$ substates may make significant contributions. The 4^- and 3^- states in ^{36}P are thus on a more equal footing and the transition probabilities to the two states are predicted to be comparable.

(c) The proton pickup takes place from the $2s_{\frac{1}{2}}$ orbit and is therefore not subject to the $j_>$ to $j_<$ preference described above.

As noted above, these arguments explain why it is that the 3^- state is populated as strongly as the 4^- state in the (^7Li,^7Be) and (^{11}B,^{11}C) reactions, whereas it is barely visible in the (^{14}C,^{14}N) spectrum. However, the prediction of the calculations that the relative intensities observed in the (^{13}C,^{13}N) and (^{14}C,^{14}N) reactions should be essentially the same is clearly not the case experimentally. Nor are the relative intensities observed in the (^{18}O,^{18}F) reaction well reproduced. In order to resolve these discrepancies, it is necessary to look to the one-step reaction mechanism.

4.3. One-Step Calculations

Full one-step **DWBA** calculations have been performed for the two reactions ($^{36}S(^{13}C,^{13}N)^{36}P$ and $^{36}S(^{18}O,^{18}F)^{36}P$) for which the ratios of the 3^-: 4^- cross-sections are not predicted correctly by the two-step calculations. These calculations were done with no free parameters and included all possible intermediate spins. For the nucleon-nucleon interaction, central and tensor terms were included, with contributions to the central term coming from both the **V0T** spin-independent and **VST** spin-dependent isovector forces. The **M3Y** interaction[20] was used with standard delta functions[21] to account for single-nucleon knock-on exchange. The energy dependence of such an interaction is only in the strength of the delta-function pseudo potential, i.e. in the Fourier transform of the knock-on exchange term evaluated at the laboratory energy. These strengths have been calculated at the present bombarding energies and were found to be $\approx$ +400 and -115 MeV fm^3, for **V0T** and **VST**, respectively. The radial wave functions of the bound states were generated from a Woods-Saxon potential with geometrical parameters $r_0 = r_c = 1.35$ fm, $a_0 = a_{so} = 0.65$ fm and $V_{so} = 7$ MeV.

The optical-potential parameters employed were those derived from the elastic scattering data and listed in table 2. The nuclear structure information, i.e. the one-body transition densities, were obtained from the shell model calculations as described above. The **DWBA** computer code used is that of ref.[22].

The results of these calculations are compared with experiment in table 5, while the relative cross-sections are compared with experiment and with the 2-step calculations in fig 5. Note that the 1-step cross-sections have been integrated over the same range of reaction angles as the experimental data.

4.3.1 Relative cross-sections

It is apparent from fig. 5 that the 1-step predictions give a much better account of the (^{13}C,^{13}N) and (^{18}O,^{18}F) data than do the 2-step, predicting correctly that the 3^- state should be strong in the former reaction and weak in the latter, whereas the 2-step calculations predict the opposite. We conclude that the 1-step mechanism is probably dominant for these two reactions at energies of 7-8 MeV/nucleon.

In both cases, however, the 1-step calculations significantly under-predict

the relative strengths of the weaker states, and the addition of a small 2-step contribution would certainly improve the quantitative agreement between experiment and prediction. Given the uncertainties in the calculations, some caution is required in drawing conclusions from such a comparison between the data and the calculations. Nevertheless, these results do suggest a contribution of a smaller, but significant, 2-step component in addition to the dominant 1-step contribution to the reaction mechanism.

For the remaining three reactions, full one-step DWBA calculations have not been carried out because optical-potential parameters were not available. However, in these cases, it is probably a reasonable approximation to evaluate the relative cross-sections from the 1-step form-factors at a typical channel radius[21] of $1.65(A_p^{1/3} + A_t^{1/3})$. The resulting 1-step relative intensities are plotted in fig. 5. Evidently, the 1-step and 2-step predictions are more or less equivalent in the cases of the $(^7Li,^7Be)$, $(^{11}B,^{11}C)$ and $(^{14}C,^{14}N)$ reactions, and in good agreement with experiment.

Hence, we conclude that the 1-step calculations give a good description of the data for all five reactions, whereas the 2-step predictions fail in just those two cases where they are qualitatively different from the 1-step. As foreshadowed earlier, this suggests strongly that the reaction mechanism of these charge-exchange reactions is dominated by 1-step processes even at these relatively low energies.

For clarity, the 2^- state at 0.43 MeV has been omitted from the above discussions. However, its behaviour is very similar to that of the 4^- ground state in both the 1-step and 2-step calculations although its strength is typically a factor of 4 weaker. Experimentally, it is observed in 4 of the 5 reactions (it is obscured by the excited state of ^{7}Be in the (^{7}Li,^{7}Be) spectrum), and does indeed follow this expectation.

Similarly, it is anticipated that the 1^- state expected at 1.6 MeV should follow the behaviour of the 3^- state, again with a factor of 4 reduction in strength, but it has not yet been observed. It falls in a region of the spectrum where it would be obscured by background due to either excited states of the ejectile, or reactions on target contaminants such as carbon and oxygen.

The physical basis of the variation in 1-step selectivity from reaction to reaction resides in the spin-dependence of the interaction as follows:

(i) Non-spin flip **V0T** components are not allowed in the transitions to the unnatural-parity 4^- and 2^- states since the the total angular momentum transferred (to the target system) must be equal to the orbital angular-momentum transferred. This implies a parity change of $(-1)^L$ which is not the case for $^{36}S(0^+) \rightarrow ^{36}P(4^-)$ (or 2^-). It follows that only the spinflip-isospin flip **VST** term can contribute to the unnatural parity transitions.

(ii) This restriction does not apply to the 3^- and 1^- states for which both **V0T** and **VST** terms may be allowed, depending on the projectile system.

(iii) The projectile system imposes no additional restrictions for ^7Li, ^{11}B, and ^{13}C, i.e. both **V0T** and **VST** terms may contribute to the transition to the 3^- state. However, the (^{14}C,^{14}N) and (^{18}O,^{18}F) reactions again involve a transition ($0^+ \rightarrow 1^+$) from natural to unnatural parity states, whence only the **VST** term can contribute in the transitions to all final states in ^{36}P.

(iv) The calculations showed that, in all cases, the spin-flip (**VST**) contribution to the cross-section of the 3^- state was an order of magnitude smaller than its contribution to the cross-section of the 4^- state. This is due to the tensor force contribution which is very important for transitions involving unnatural parity states (see for instance ref.[20]).

(v) The variation from one reaction to another arises, therefore, from the non-spin-flip (**V0T**) contribution (or lack of it) to the 3^- state. In those cases where it is allowed, it is found to dominate the cross-section of the 3^- state, and, as noted above, these are precisely the cases for which the 3^- is found experimentally to be populated with a strength greater than or equal to the 4^- state, i.e. for the reactions involving the ^7Li, ^{11}B, and ^{13}C beams.

4.3.2. Absolute cross-sections.

In contrast to the 2-step calculations, the 1-step calculations yield absolute cross sections which can be compared with experiment. Such a comparison is made in table 5 for the two reactions for which optical model parameters are available and hence for which the calculations are possible. Clearly, the calculations underestimate the cross-sections in all four cases, although the normalisation factors for the strongest state in each reaction are comparable. As noted above, the rather larger normalisation factors for the weaker states may point to some 2-step contribution.

Normalisation factors of this order are common in the DWBA analyses

of heavy-ion induced transfer reactions involving the transfer of 2 nucleons. This is due in part to the neglect of higher-order reaction mechanisms which add coherently to the two mechanisms considered here. In addition, it is well known that the magnitudes of these calculated cross-sections are sensitive to details of the calculations such as the strength and form of the interaction and the parameters of the distorted wave calculations. Often, as is the case here, there is little choice but to use the same optical model potentials in the entrance and exit channels even though different nuclei are involved. Hence, the calculated absolute cross sections are probably not a reliable indicator of the relative importance of the 1-step reaction mechanism at these energies. On the other hand, the relative cross sections for the various final states in ^{36}P are determined predominantly by selection rules and are therefore insensitive to the details of the calculations. Hence, the comparison of these relative cross-sections with experiment which was made above is probably a more reliable indicator of the relative importance of one-step and two-step reaction modes at these energies.

V. CONCLUSION

New experimental data for a series of charge-exchange reactions on ^{36}S targets at energies of $\sim$7 MeV/A have been obtained and analysed in the present work. Calculations of the relative cross-sections for final states in ^{36}P have been performed for both one-step and two-step pictures of the reaction mechanism. In two cases, i.e. the $^{36}S(^{13}C,^{13}N)^{36}P$ and $^{36}S(^{18}O,^{18}F)^{36}P$ reactions, the predictions were sufficiently different from each other to favour clearly the 1-step mechanism. In the remaining three cases, both the 1-step and 2-step calculations were in reasonable agreement with experiment. Since the 1-step predictions give a good account of the data for all five reactions, whereas the 2-step prescription fails for just those two cases where its predictions differ from the 1-step, we conclude that these charge-exchange reactions most likely proceed predominantly by a 1-step mechanism, even at the comparatively low energies employed in the present work.

We would like to thank Dr. B. A. Brown for kindly sending us the SDPF interaction. This work was supported in part by the Consejo Nacional de

Investigaciones Científicas y Técnicas, Argentina.

* On leave at Fermi National Accelerator Laboratory, Batavia, Ill 60563, USA.

References

[1] J.S.Winfield, N.Anantaraman, S.M.Austin, Ziping Chen, A.Galonsky, J.van der Plicht, H.L.Wu, C.C.Chang and G.Ciangaru, Phys. Rev. **C35**(1987)1734

[2] W. von Oertzen, Nucl. Phys. **A482**(1988)357c

[3] J.Cook, K.W.Kemper, P.V.Drumm, L.K.Fifield, M.A.C.Hotchkis, T.R.Ophel and C.L.Woods, Phys. Rev. **C30**(1984)1538

[4] N.Anantaraman, J.S.Winfield, S.M.Austin, J.A.Carr, C.Djalali, A.Gillibert, W.Mittig, J.A.Nolen and Zhan Wen Long, Phys. Rev. **C44**(1991)398

[5] J.S. Winfield, N. Anantaraman, Sam M. Austin, L.H. Harwood, J. van Plicht, H.L. Wu, and A.F. Zeller, Phys. Rev. **C33**(1986)1333

[6] F. Petrovich in *The (p,n) Reaction and the Nucleon-Nucleon Force*, edited by C.D. Goodman, Sam M. Austin, S.D. Bloom, J. Rapaport, and G.R. Satchler, (Plenum, New York, 1980) p. 135.

[7] A. Etchegoyen, M.C. Etchegoyen, E.D. Izquierdo, D. Abriola, D.E. Di-Gregorio, J.O. Fernández Niello, A.M.J. Ferrero, S.Gil, A.O. Macchiavelli, A.J. Pacheco, and J.E. Testoni, Phys. Rev **C38** (1988)2124

[8] P.V.Drumm, L.K.Fifield, R.A.Bark, M.A.C.Hotchkis, C.L.Woods and P.Maier-Komor, Nucl. Phys. **A441**(1985)95

[9] W.A.Mayer, W.Henning, R.Holzwarth, H.J.Körner, G.Korschinek, W.U.Mayer, G.Rosner and H.J.Scheerer, Z.Phys. **A319**(1984)287

[10] J.P.Dufour, R. Del Moral, A.Fleury, F.Hubert, D.Jean, M.S.Pravikoff, H.Delagrange H.Geissel and K.-H.Schmidt, Z.Phys. **A324**(1986)487

[11] L.K.Fifield and N.A.Orr, Nucl. Instr. and Meth., **A288**(1990)360

[12] C. Thibault et al., Phys. Rev. **C12**, 644 (1975). C. Détraz et al., Nucl. Phys. **A426**, 37 (1984). G.W. Butler et al., Phys. Rev. Lett., **38**(1987)1380

[13] E. K. Warburton, D. E. Alburger, J. A. Becker, B. A. Brown, and S. Raman, Phys. Rev. **C34**(1986)1031

[14] S. Cohen and D. Kurath, Nucl. Phys. **A73**(1965)1

[15] B. H. Wildenthal, Prog. Part. Nucl. Phys, **11**(1984)5

[16] A. Etchegoyen, W. D. M. Rae, and N. S. Godwin (MSU version: B. A. Brown, W. E. Ormand, and J. S. Winfield), "The Oxford-Buenos Aires Shell-Model Code", (unpublished).

[17] W. K. Warburton and J. A. Becker, Phys. Rev. **C35**(1987)1851

[18] W.N.Catford, L.K.Fifield, N.A.Orr and C.L.Woods, Nucl. Phys. **A503**(1989)263

[19] D.M.Brink, Phys. Lett. **B40**(1972)935

[20] G. Bertsch, J. Borysowich, A. McManus, and W. G. Love, Nucl. Phys. **A284**(1977)399

[21] M. Golin, F.Petrovich, and D. Robson, Phys. Lett., **B64** (1976)253

[22] A. Etchegoyen and M. C. Etchegoyen, Comp. Phys. Comm., **55** (1989)217

Table 1. Experimental Parameters

Beam	Energy (MeV)	Reaction Angle	Angular Acceptance	Laboratory
^{7}Li	54	10°	4.5°	ANU[a]
^{11}B	81	10°	4.5°	ANU[a]
^{13}C	94.5	8°	4.5°	ANU[a]
^{14}C	71	10°		Munich[b]
^{18}O	124	8°	4.5°	ANU[a]

[a] Present work
[b] Ref.[9]

Table 2. Measured Cross Sections

Reaction	Cross Section (mb/sr)		
	g.s. (4^-)	0.25 MeV (3^-)	0.42 MeV (2^-)
$^{36}S(^{7}Li,^{7}Be)^{36}P$	0.26	0.25	<0.08
$^{36}S(^{11}B,^{11}C)^{36}P$	0.13	0.12	0.01
$^{36}S(^{13}C,^{13}N)^{36}P$	0.09	0.14	0.04
$^{36}S(^{14}C,^{14}N)^{36}P$[a)]	0.40	<0.03	0.07
$^{36}S(^{18}O,^{18}F)^{36}P$	0.50	0.13	0.10

a) Ref.[9)]

Table 3. Optical model parameters

	Energy (MeV)	V (MeV)	a (fm)	r_0 (fm)	W_{sd} (MeV)	a_{sd} (fm)	r_{sd} (fm)	r_c (fm)
$^{13}C + ^{36}S$	98	92.8	1.466	0.524	12.9	0.766	1.107	1.2
$^{18}O + ^{36}S$	112	88.6	1.427	0.449	62.7	1.002	0.775	1.2

The radius parameters r_0, r_{sd} and r_c follow the heavy-ion convention. The subscript "sd" indicates a surface-derivative imaginary potential.

Table 4. Average no of particles in each j-level

	$1d_{5/2}$	$1d_{3/2}$	$2s_{1/2}$	$1f_{7/2}$	$1f_{5/2}$	$2p_{3/2}$	$2p_{1/2}$
$^{36}S(0+, g.s.)$	11.83	4.39	3.78	-	-	-	-
$^{36}P(4^-, g.s.)$	11.75	4.25	3.00	0.99	0.00	0.00	0.00
$^{36}P(3^-, 0.13\ MeV)$	11.75	4.33	2.92	0.95	0.01	0.04	0.00
$^{36}P(2^-, 0.66\ MeV)$	11.80	4.55	2.65	0.39	0.00	0.61	0.00
$^{36}P(1^-, 1.56\ MeV)$	11.73	4.23	3.04	0.05	0.00	0.91	0.03

Occupation numbers lower than 0.005 have been set to zero.

Table 5. Calculated 1-step cross-sections in the laboratory frame

Reaction	Scattering Angle	Theory (mb/sr)	Exper. (mb/sr)	N[a]	V0T (mb/sr)	VST (mb/sr)
$^{36}S(^{18}O,^{18}F)^{36}P(4^-)$	8	0.066	0.50	7.6	-	0.066
$^{36}S(^{18}O,^{18}F)^{36}P(3^-)$	8	0.006	0.13	22	-	0.006
$^{36}S(^{13}C,^{13}N)^{36}P(4^-)$	8	0.010	0.09	9.0	-	0.010
$^{36}S(^{13}C,^{13}N)^{36}P(3^-)$	8	0.036	0.14	3.9	0.035	0.001

[a] The normalisation factor, N, corresponds to the ratio of the experimental to the theoretical cross section. In the two cases for which N is given, the experimental cross-section is believed to be dominated by the 1-step component, although this is a better assumption for the (^{13}C,^{13}N) reaction than for the (^{18}O,^{18}F) reaction (see text).

Figure Captions

Figure 1
Spectra of charge-exchange reactions on ^{36}S targets. Peaks corresponding to low-lying levels in ^{36}P are labelled with J^{π}. The 4^- state is the ground state, while the 3^- and 2^- states are at excitation energies of 0.25 and 0.43 MeV respectively. Peaks labelled with an asterisk are due to excitation of excited states of the ejectile, and those labelled ^{16}N are due to charge exchange reactions on ^{16}O in the target. The (^{14}C,^{14}N) spectrum was derived from ref.[9].

Figure 2
Angular distributions of ^{13}C and ^{18}O ions elastically scattered from a ^{36}S target at energies of 98 and 112 MeV respectively. The solid lines are the optical model fits.

Figure 3
Comparison of experimental relative intensities with the results of 2-step calculations for five different charge-exchange reactions on ^{36}S targets. The relative intensities have been normalised to the 4^- ground state. The (^{14}C,^{14}N) data are from ref.[9] and the experimental value for the 3^- state represents an estimated upper limit. The absence of an experimental value for the 2^- state in the (^{7}Li,^{7}Be) frame is due to the presence in the spectrum of the 0.43 MeV excited state of ^{7}Be.

Figure 4
Schematic representation of the 2 steps leading to the preferential population of the 4^- state in ^{36}P by the ^{36}S(^{13}C,^{13}N)^{36}P reaction. The z-projections of the angular momenta of the various nucleons participating in the reaction are indicated.

Figure 5
Comparison of experimental relative intensities with the results of both 1-step and 2-step calculations for five different charge-exchange reactions on ^{36}S targets. The relative intensities have been normalised to the 4^- ground state. The (^{14}C,^{14}N) data are from ref.[9] and the experimental value for the 3^- state represents an estimated upper limit.

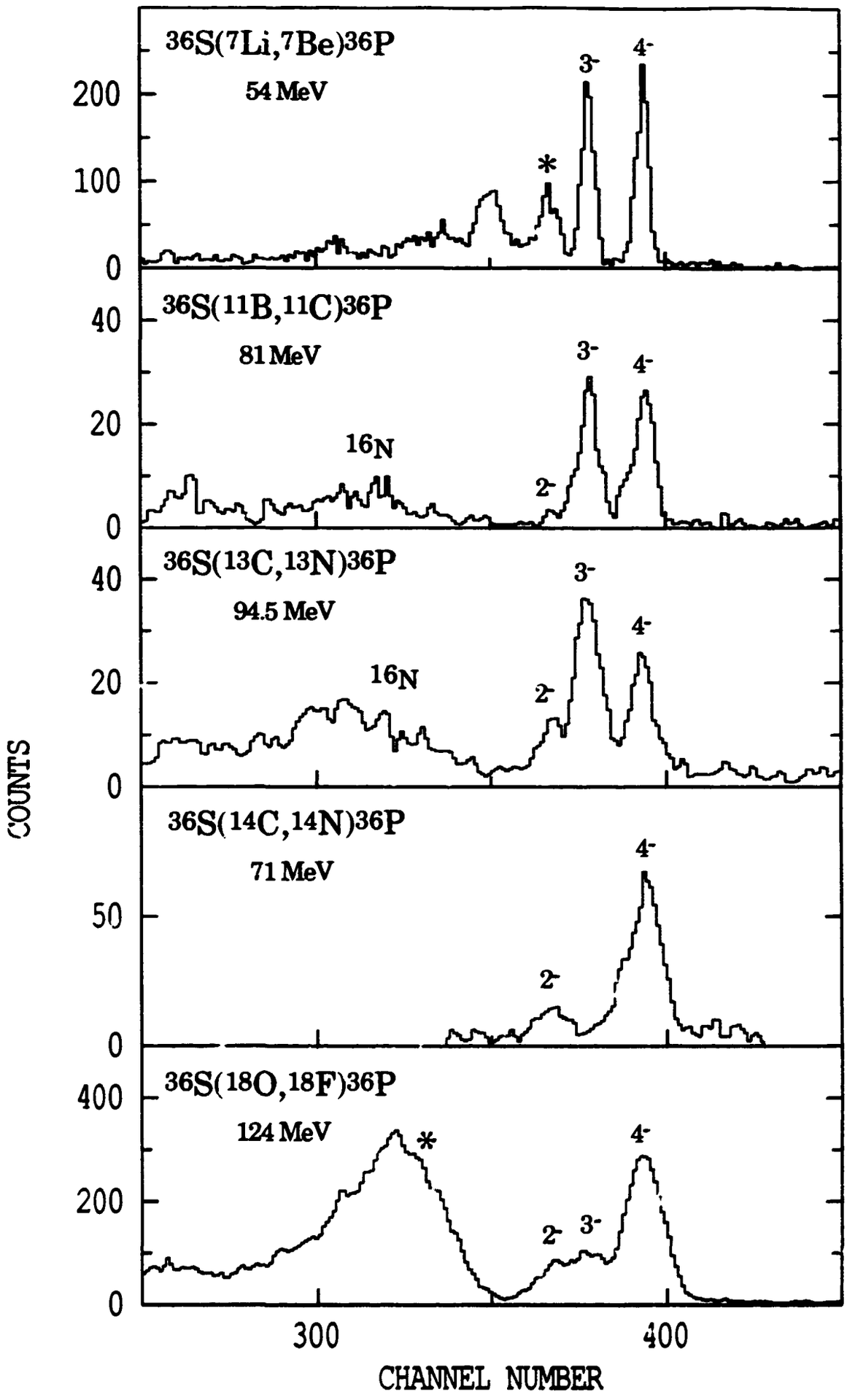
36S(7Li,7Be)36P
54 MeV
3-
4-
*
200
100
0
36S(11B,11C)36P
81 MeV
3-
4-
16N
2-
40
20
0
36S(13C,13N)36P
94.5 MeV
3-
4-
16N
2-
40
20
0
36S(14C,14N)36P
71 MeV
4-
2-
50
0
36S(18O,18F)36P
124 MeV
*
4-
2-
3-
400
200
0
COUNTS
300
400
CHANNEL NUMBER

Fig. 1

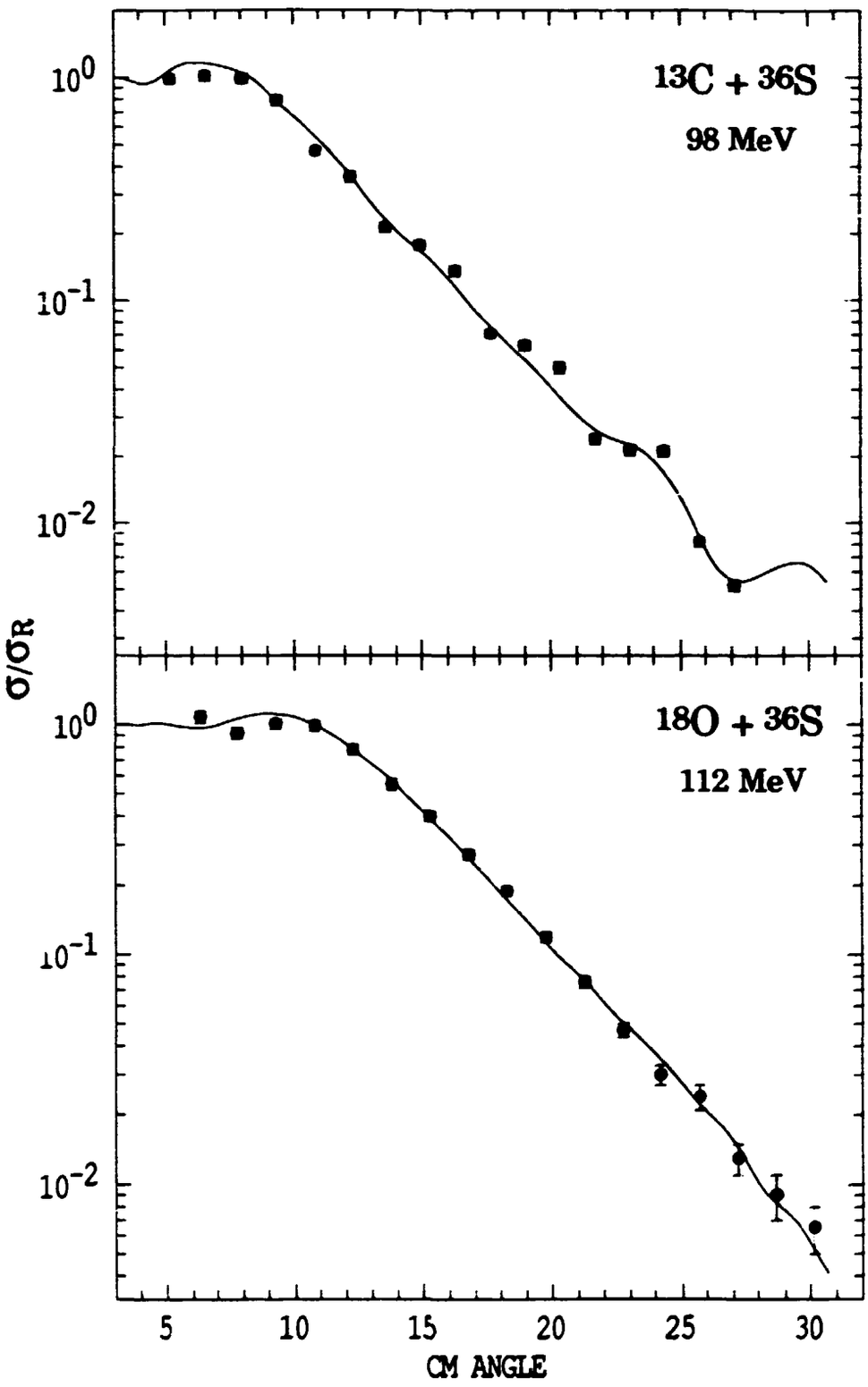
$^{13}C + ^{36}S$
98 MeV
$^{18}O + ^{36}S$
112 MeV
10^0
10^{-1}
10^{-2}
σ/σ_R
5
10
15
20
25
30
CM ANGLE

Fig. 2

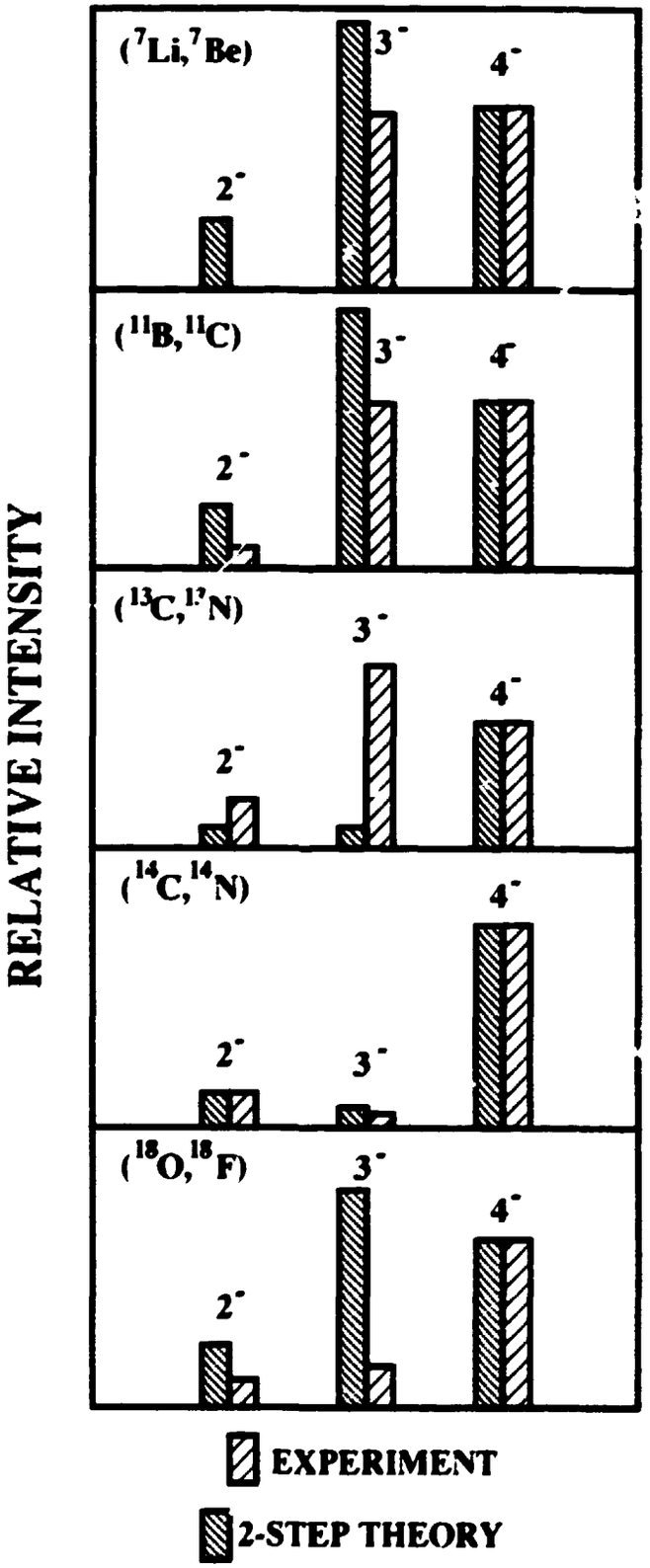
RELATIVE INTENSITY
(^{7}Li,^{7}Be)
2^{-}
3^{-}
4^{-}
(^{11}B,^{11}C)
2^{-}
3^{-}
4^{-}
(^{13}C,^{13}N)
2^{-}
3^{-}
4^{-}
(^{14}C,^{14}N)
2^{-}
3^{-}
4^{-}
(^{18}O,^{18}F)
2^{-}
3^{-}
4^{-}
EXPERIMENT
2-STEP THEORY

Fig. 3

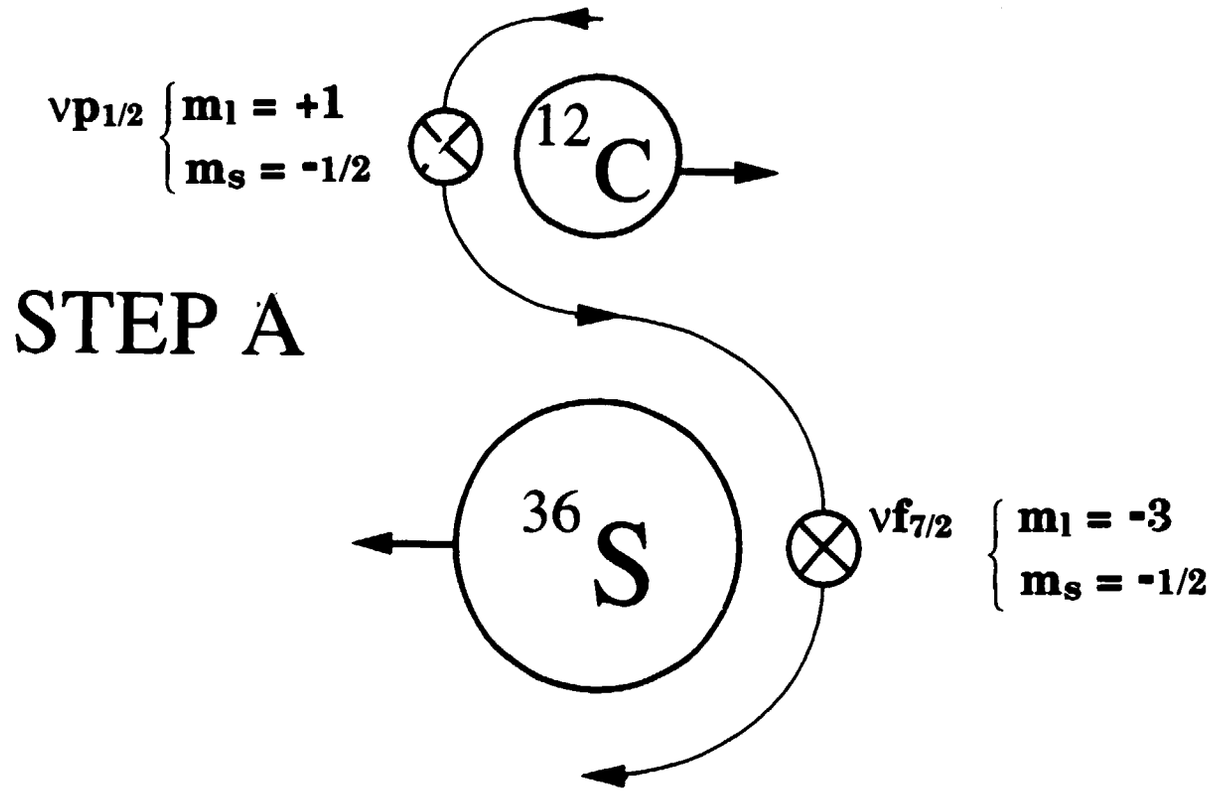
νp1/2 { ml = +1
ms = -1/2
12C
STEP A
36S
νf7/2 { ml = -3
ms = -1/2

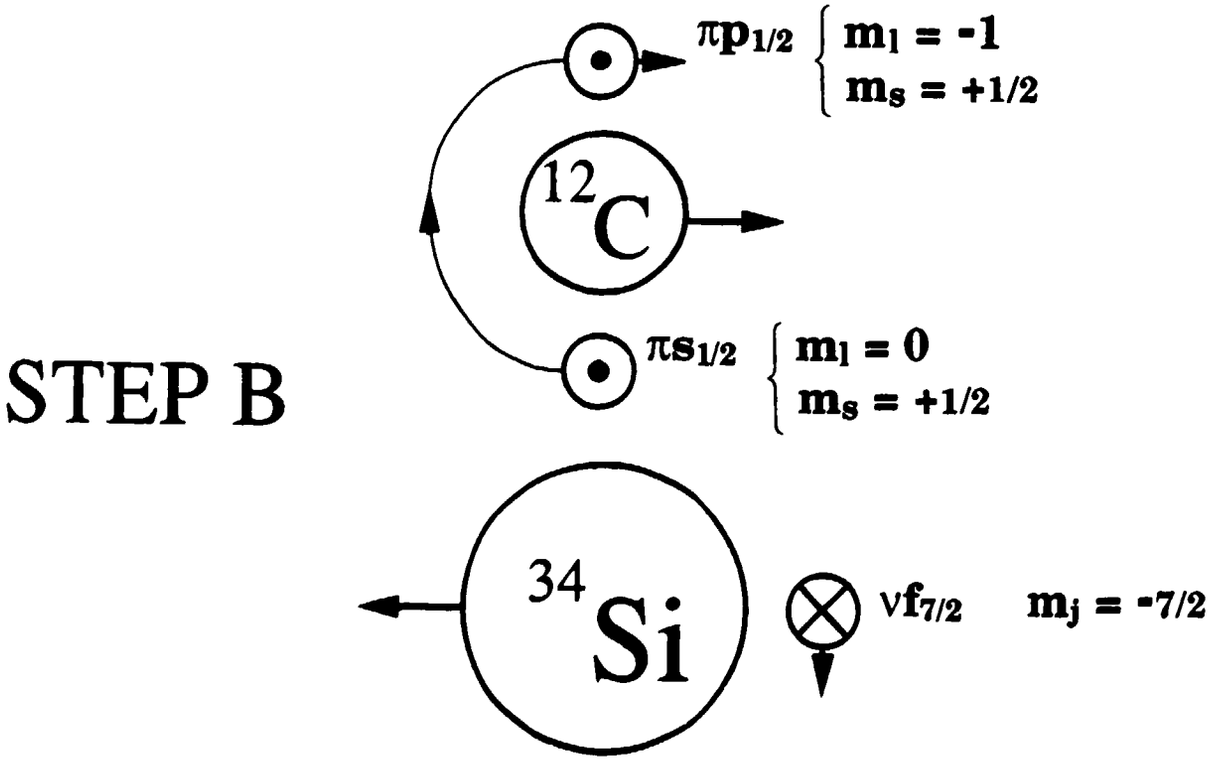
πp1/2 { ml = -1
ms = +1/2
12C
πs1/2 { ml = 0
ms = +1/2
STEP B
34Si
νf7/2 mj = -7/2
πs1/2 { ml = 0
ms = -1/2

Fig. 4

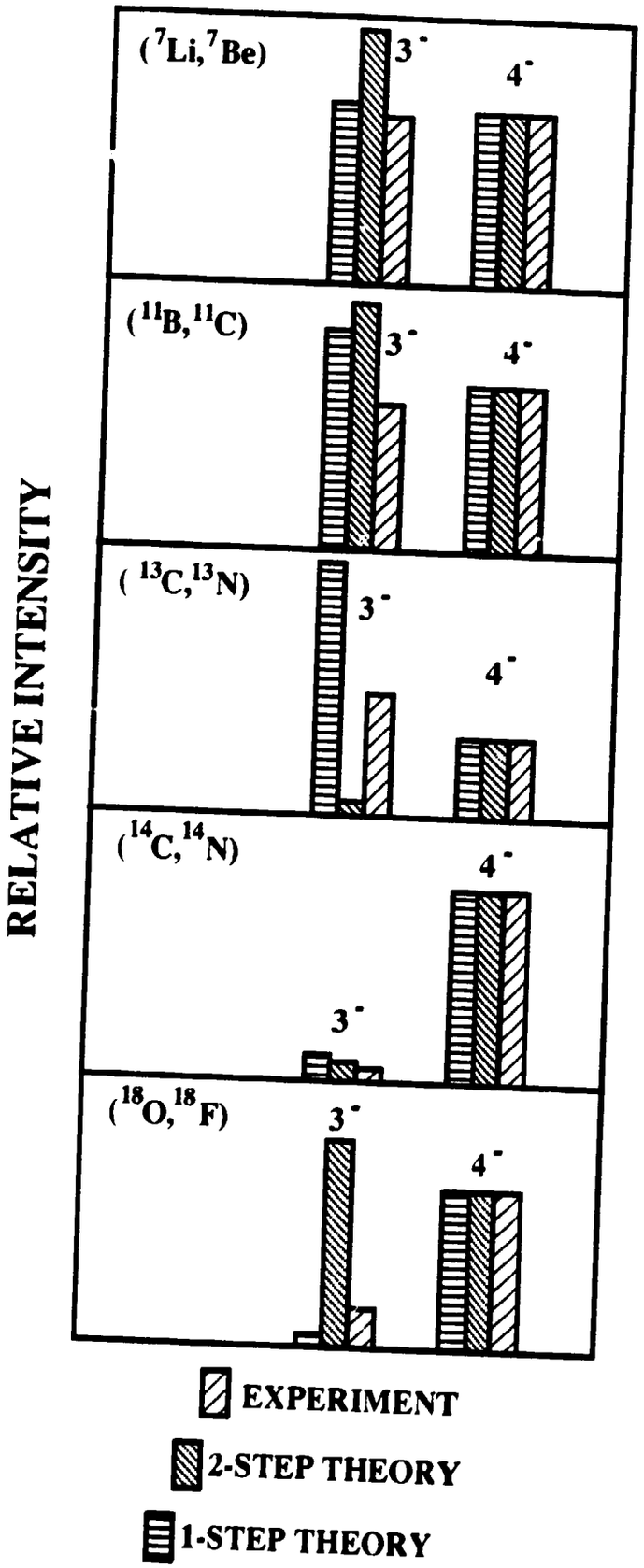
RELATIVE INTENSITY
(^{7}Li,^{7}Be)
3$^-$
4$^-$
(^{11}B,^{11}C)
3$^-$
4$^-$
(^{13}C,^{13}N)
3$^-$
4$^-$
(^{14}C,^{14}N)
4$^-$
3$^-$
(^{18}O,^{18}F)
3$^-$
4$^-$
EXPERIMENT
2-STEP THEORY
1-STEP THEORY

Fig. 5